Hindawi
International Journal of Photoenergy
Volume 2021, Article ID 6623150, 8 pages
https://doi.org/10.1155/2021/6623150

*Research Article*

# Role of Interfacial Oxide Layer in $MoO_x$/*n*-Si Heterojunction Solar Cells

**X. M. Song**,[1,2] **Z. G. Huang**,[2] **M. Gao**,[1] **D. Y. Chen**,[1] **Z. Fan**,[2] **and Z. Q. Ma**[1,3]

[1]*SHU-SolarE R&D Lab, Department of Physics, College of Science, Shanghai University, 200444, China*
[2]*School of Science, Jiangsu Ocean University, 222005, China*
[3]*Instrumental Analysis & Research Center, Shanghai University, 200444, China*

Correspondence should be addressed to Z. Q. Ma; zqma@mail.shu.edu.cn

Received 29 November 2020; Revised 21 March 2021; Accepted 10 April 2021; Published 23 April 2021

Academic Editor: Yuanzuo Li



Interfacial oxide layer plays a crucial role in a $MoO_x$/*n*-Si heterojunction (MSHJ) solar cell; however, the nature of this interfacial layer is not yet clarified. In this study, based on the experimental results, we theoretically analyzed the role of the interfacial oxide layer in the charge carrier transport of the MSHJ device. The interfacial oxide layer is regarded as two layers: a quasi *p*-type semiconductor interfacial oxide layer ($SiO_x$(Mo))1 in which numerous negatively charged centers existed due to oxygen vacancies and molybdenum–ion-correlated ternary hybrids and a buffer layer ($SiO_x$(Mo))2 in which the quantity of Si-O bonds was dominated by relatively good passivation. The thickness of ($SiO_x$(Mo))1 and the thickness of ($SiO_x$(Mo))2 were about 2.0 nm and 1.5 nm, respectively. The simulation results revealed that the quasi *p*-type layer behaved as a semiconductor material with a wide band gap of 2.30 eV, facilitating the transport of holes for negatively charged centers. Additionally, the buffer layer with an optical band gap of 1.90 eV played a crucial role in passivation in the $MoO_x$/*n*-Si devices. Furthermore, the negative charge centers in the interfacial layer had dual functions in both the field passivation and the tunneling processes. Combined with the experimental results, our model clarifies the interfacial physics and the mechanism of carrier transport for an MSHJ solar cell and provides an effective way to the high efficiency of MSHJ solar cells.

## 1. Introduction

As a novel structure for a silicon-based solar cell, selective passivated contact has attracted much attention in recent years due to its successful transport of majority charge carriers and the reduction of the recombination rate of minority charge carriers [1–7]. Among the transition metal oxide thin films, substoichiometric molybdenum oxide ($MoO_x$, $0 < x < 3$) has previously been reported as an effective hole-collecting material for solar cells [4, 7–11]. $MoO_x$ thin films were recently directly integrated into silicon-based heterojunction (SHJ) devices, and a photovoltaic (PV) feature was successfully obtained due to the appropriate band gap of ~3.00 eV and the higher work function [6, 12]. Furthermore, the SHJ device showed an excellent photovoltaic (PV) performance [3, 4, 13].

$MoO_x$ combines a wide bandgap with a high work function, which makes it possible to provide an excellent hole-selective function. It has been reported that a 7 nm-thick $MoO_x$ film has been used to replace the a-Si:H(*p*) layers in SHJ devices, resulting in a conversion efficiency of 22.5% [13]. We demonstrated a different $MoO_x$/n-Si SHJ solar cell with an efficient hole collection and simple fabrication process by evaporating $MoO_3$ powder onto an *n*-type silicon. A 3.5 nm-thick amorphous interfacial layer formed naturally was observed between the $MoO_x$ film and the *n*-Si substrate via high-resolution transmission electron microscopy (HRTEM). Although the high work function of the $MoO_x$ layer induced an interfacial inversion layer in the surface of the *n*-Si substrate, forming the build-in-potential, it was not negligible that the 3.5 nm interfacial oxide layer also played a significant role in the transport of carriers.

In this research, we achieved an $\eta$ of 13.94% for an MSHJ solar cell by employing this simple process, as well as a $V_{oc}$ of 569.96 mV, an $J_{sc}$ of 32.10 mA·cm$^{-2}$, and a fill factor (FF) of 76.21%. To determine the optoelectrical properties of the

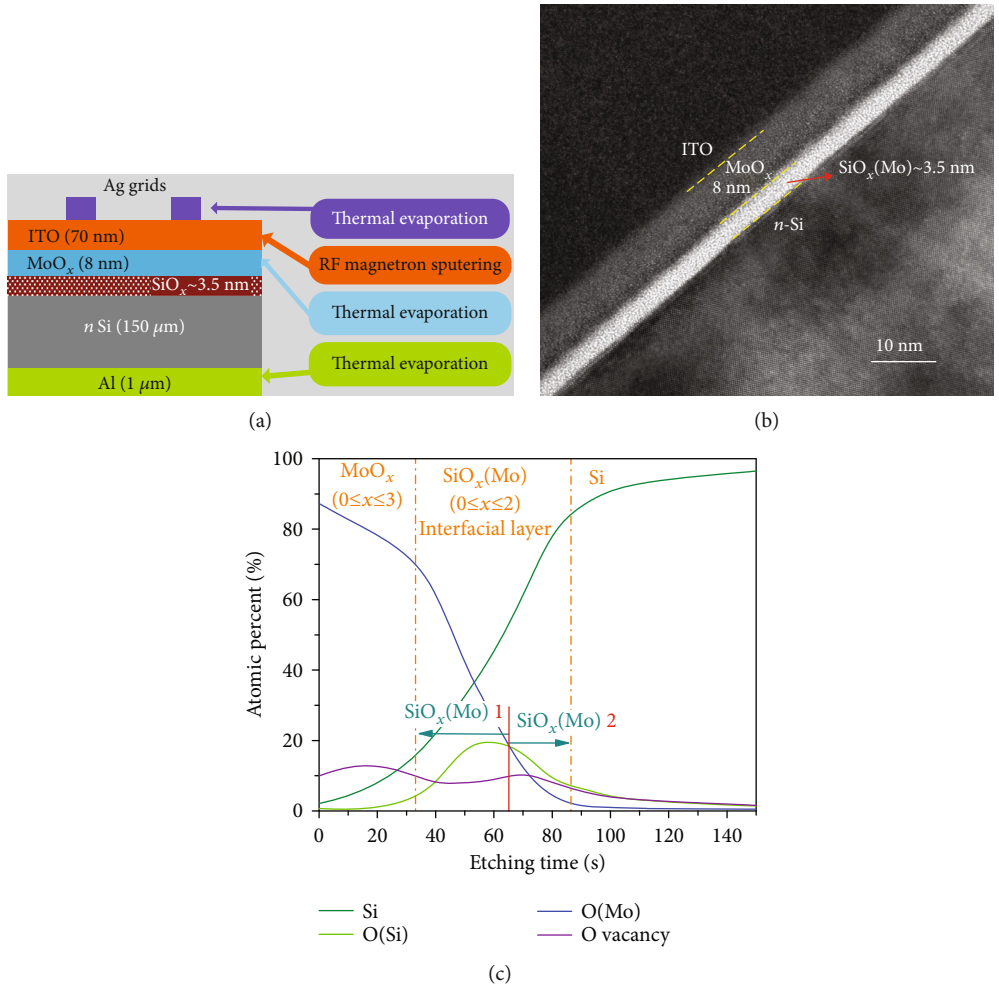


FIGURE 1: (a) Schematic of the MSHJ solar cell structure. (b) The cross-sectional HRTEM image of the interfacial layer of the $MoO_x$/*n*-Si. (c) Relative atomic percentage distribution of O (Si) (denotes O-Si bond), O (Mo) (denotes O-Mo bond), and Si with an increasing etching time for the transitional region between the $MoO_x$ film and the *n*-Si substrate.

interfacial layer, we used AFORS-HET v2.5 to model and implement the reconstruction of the interfacial layer [14]. This interfacial layer was regarded as two layers, including a quasi *p*-type semiconductor interfacial oxide layer ($SiO_x$(Mo))1 and a buffer layer ($SiO_x$(Mo))2. In detail, the quasi *p*-type layer was a semiconductor material that facilitated the transport of holes. At the same time, the buffer layer played the role of chemical passivation for the $MoO_x$/*n*-Si devices. Importantly, the negative charge centers in the interfacial layer had dual functions in both the field-effect passivation and the tunneling processes. Finally, we numerically achieve an $\eta$ of 16.91% for an MSHJ combined with advanced light trapping textures and rear surface passivation. The simulation results help us achieve an effective way to the high efficiency from the clarification of the interfacial physics in the MSHJ solar cells.

## 2. Simulation Model

A schematic of the MSHJ solar cell is shown in Figure 1(a). An amorphous interfacial layer with a thickness of approximately 3.5 nm, as shown in Figure 1(b), was naturally formed between the $MoO_x$ and the *n*-Si substrate during the evaporation of the $MoO_x$, as confirmed by cross-sectional HRTEM imaging. X-ray photoelectron spectroscopy (XPS) with depth profiling was used to determine the elemental composition of the interfacial layer, as shown in Figure 1(c). One could find that Si, O, and Mo were the constituents of the interfacial transition. Except for the measured thickness and the elemental composition, there was no other direct observation of the -$SiO_x$(Mo) interface because the interface was ultrathin and located inside of the structure. However, the role of *a* the *a*-$SiO_x$(Mo) layer in the MSHJ was not yet clear. To understand the nature of the interfacial layer, we constructed a physical model and simulated the optical and electrical properties of the *a*-$SiO_x$(Mo) layer in the AFORS-HET v2.5 software. The intraband and Schottky barrier tunneling through the spikes in the conduction and valence bands that occurred at interfaces were also considered.

In our previous studies [15, 16], we calculated a periodic *a*-$SiO_2$ structure with Mo doping by using first-principles calculations to explain the mechanism of charge carrier

Table 1: Simulation parameters of the interfacial layer in the MSHJ solar cell.

| Parameter | Quasi-$p$-$a$-$SiO_x$ (Mo) | Quasi-$i$-$a$-$SiO_x$ (Mo) | $N$-$c$-Si |
|---|---|---|---|
| Layer thickness (cm) | $2.0 \times 10^{-7}$ | $1.5 \times 10^{-7}$ | $1.5 \times 10^{-2}$ |
| Electron affinity (eV) | 3.50 | 3.50 | 4.05 |
| Mobility gap (eV) | Variable | Variable | 1.12 |
| Optical gap (eV) | Variable | Variable | 1.12 |

transport. The results showed that the charge transition levels of $\varepsilon$ (+1/0) and $\varepsilon$ (+2/0) existed, and that these levels were located at 3.59 eV and 2.54 eV, respectively, above the valence band maximum of $a$-$SiO_2$. These charge transition levels introduced a number of negative charge centers that lowered the tunneling barrier height. We surmised that the charge carrier transport in the interfacial layer was also applicable to the one-dimensional semiconductor equations in the steady state. It was feasible to implement this simulation by using the AFORS-HET v2.5 software.

According to the relative atomic percentage distribution of O(Si) (denotes O-Si bond) and O(Mo) (denotes O-Mo bond) shown in Figure 1(c), the Mo-O and Si-O bonds show two different distributions near the $MoO_x$ layer and Si substrate. Therefore, we divided the interfacial layer into two physical layers: one layer was regarded as a 2 nm-thickness quasi $p$-type $SiO_x$(Mo)1 layer because the quantity of the Mo-O bond is larger than that of the Si-O bond near the $MoO_x$ film. The other layer was a 1.5 nm-thickness quasi $i$-type ($SiO_x$(Mo)2) since the Si-O bond was greater than the Mo-O bond near the Si substrate.

The 8.0 nm-thick $MoO_x$ layer was modeled as a portion of a composite transparent conductive oxide [3]. Its work function was set to 5.50 eV [16], which was determined from UPS. Moreover, the reflection and the absorption at the front surface were extracted from data measured with an ultraviolet-visible spectrophotometer. The average density of state for the interfacial layer was set to $1.2 \times 10^{11}$ $eV^{-1} \cdot cm^{-2}$, which was measured with the special cyclic voltammetry technique reported in our previous work [17]. Carrier transport across the $a$-$SiO_x$(Mo)/$c$-Si interface was described by a thermionic emission model with active tunneling at the interface. The surface recombination velocities of the electrons and holes at the front and rear surfaces were set to the same value of $1 \times 10^7$ $cm \cdot s^{-1}$ [18–21]. The photovoltaic characteristics of the solar cells were calculated for an air mass 1.5 (AM1.5) solar spectrum (100 $mW \cdot cm^{-2}$) at room temperature. The relevant parameters are listed in Table 1. More details regarding the simulation parameters for different layers of the device can be found in our previously published study [22].

## 3. Results and Discussion

*3.1. Comparison of the Fabricated MSHJ Performance and Simulated Results.* Figure 2 shows a comparison of the simulated and measured $J$–$V$ curves of the MSHJ solar cell. The $\eta$ of the simulation results was 16.91%, together with a $J_{sc}$ of 35.72 $mA \cdot cm^{-2}$, a $V_{oc}$ of 581.10 mV, and an FF of 81.45%, which represented a better performance than that of the fabricated MSHJ with an $\eta$ of 13.94%, a $J_{sc}$ of 32.10 $mA \cdot cm^{-2}$, a $V_{oc}$ of 569.96 mV, and an FF of 76.21%. Despite the better theoretical performance, the simulated $J$–$V$ curve agreed with the measured curve, which guaranteed that the simulated $J$–$V$ curve reflected the experimental results well.

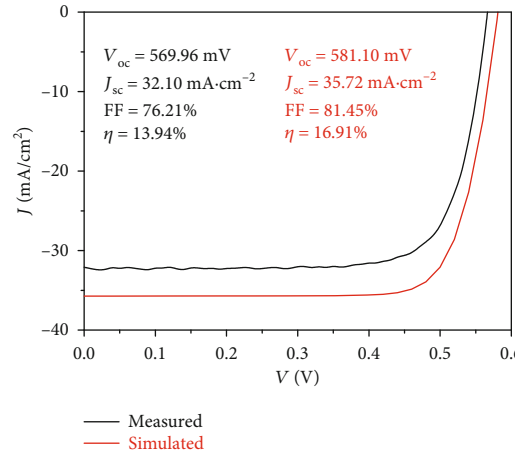


Figure 2: Current density versus voltage ($J$–$V$) curves of the measured MSHJ solar cell and the simulated model.

*3.2. Optical Band Gap of the a-$SiO_x$(Mo) Interlayer.* Figure 3 shows the $J$–$V$ characteristics for the simulated MSHJ solar cells with different energy band gap ($E_g$) values and different electron affinities for the $SiO_x$(Mo)1 and $SiO_x$(Mo)2 compared to the experimental solar cell with AM1.5 illumination. As shown in Figures 3(a) and 3(b), the simulated $J$–$V$ plot of the $SiO_x$(Mo)1 for an optical band gap of ~2.30 eV (±0.02 eV) and an electron affinity of 3.50 eV (±0.05 eV) had the good agreement with the experimental data of the MSHJ solar cell according to the shapes of $J$-$V$ curses. Table 2(a) shows photovoltaic characteristics of the $MoO_x$/$n$-Si solar cells with different band gaps of the $SiO_x$(Mo)1 layer. One can find that $V_{oc}$ and $J_{sc}$ had no a sensible change while band gap of $SiO_x$(Mo)1 varied. By comparison, it had relatively obvious impact on FF (Fill factor). A simulated FF of ~81.45% was close to 76.21% of the PV device for optical band gap of ~2.30 eV (±0.02 eV) in spite of the idealized approximation on interface states. Meanwhile, a simulated $\eta$ of ~16.91% was near 13.94% of solar cell in practice. Table 2(b) shows photovoltaic characteristics of the $MoO_x$/$n$-Si solar cells with affinity of the $SiO_x$(Mo)1 layer. The same condition also applied to the affinity of the $SiO_x$(Mo)1 layer. The $J$-$V$ plot with an affinity of ~3.50 eV (±0.05 eV) similar had the ideal agreement due to FF and $\eta$.

Figures 3(c) and 3(d) show the comparison of the different energy band gap values and the different electron affinities of $SiO_x$(Mo)2. The figure also displays the fact that the $V_{oc}$ and $J_{sc}$ hardly experienced changes with the energy band gap and the electron affinity of the $SiO_x$(Mo)2 layer, but FF and $\eta$ varied greatly while the energy band gap and the electron affinity of $SiO_x$(Mo)2 changed. And It could be found

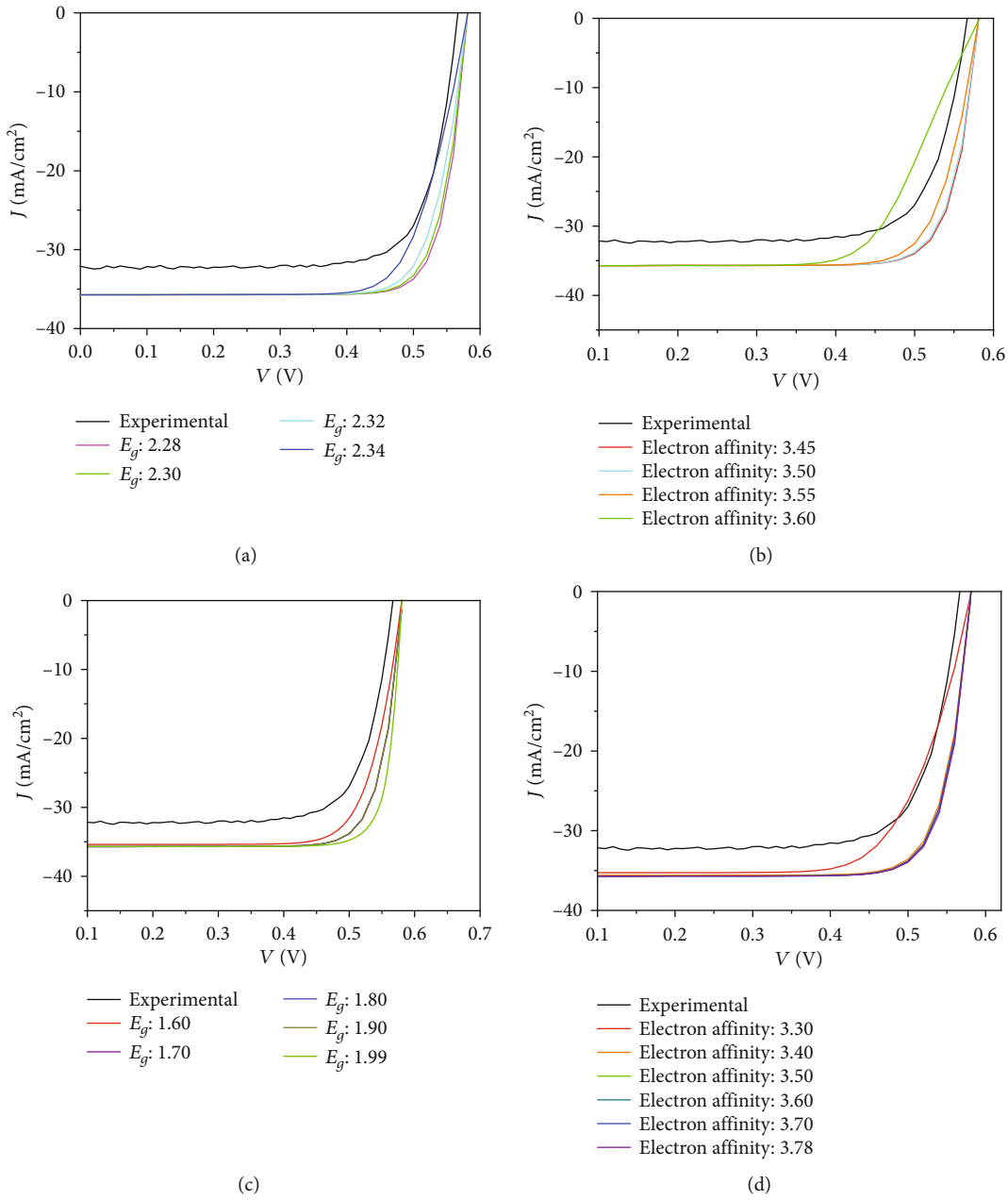


Figure 3: Comparison between the $J$–$V$ curves of the simulated MSHJ solar cells with (a) different optical $E_g$ of $SiO_x$(Mo)1, (b) different optical $E_g$ of $SiO_x$(Mo)2, (c) different affinities of $SiO_x$(Mo)1, and (d) different affinities of $SiO_x$(Mo)2 and the experimental results.

that the $J$–$V$ curve with the energy band gap of ~1.90 eV (±0.10 eV) and the electron affinity of ~3.60 eV(±0.20 eV) agreed well with the measured $J$-$V$ plot.

The energy barriers for the electrons and holes were determined by the band gap and the electron affinity. As noted in the literature [23], the FF was influenced by the series resistance, which was closely related to the energy gap. A larger gap for the same electron affinity indicated a higher barrier, thereby producing a bigger series resistance that showed a lower FF. It is well known that the optical band gap of the $a$-$SiO_x$(Mo) layer, which directly influences the transport of carriers, plays an essential role in the performance of the $MoO_x$/$n$-Si heterostructure. Nicolae Tomozeiualso discussed the optical band gap of the $SiO_x$ ($0 \le x \le 2$) in their O'Leary–Johnson–Lim (OJL) model, reporting that the optical band gap of $a$-$SiO_x$ increased from 1.7 eV to 3.1 eV as $x$ increased from 0.35 to 1.43 [24]. Therefore, it was reasonable for the $a$-$SiO_x$(Mo)1 interlayer to have an optical band gap of 2.30 eV. The band gap of the $a$-$SiO_x$(Mo)2 interlayer nearer to the Si substrate, ~1.90 eV, was slightly lower than that of the $a$-$SiO_x$(Mo)2 interlayer because of the higher Si atom content.

*3.3. Role of the Negative Charge Centers.* Another crucial problem of the interfacial layer was the concentration of negative charge centers associated with oxide vacancies and Mo–

Table 2

(a) Photovoltaic characteristics of the $MoO_x$/$n$-Si solar cells with different band gaps of the $SiO_x$(Mo)1 layer

| Band gap of $SiO_x$(Mo)1 (eV) | $V_{oc}$ (mV) | $J_{sc}$ (mA·cm$^{-2}$) | FF (%) | $\eta$ (%) |
|---|---|---|---|---|
| 2.28 | 581.1 | 35.73 | 81.67 | 16.96 |
| 2.30 | 581.1 | 35.72 | 81.45 | 16.91 |
| 2.32 | 581.2 | 35.72 | 80.97 | 16.81 |
| 2.34 | 581.3 | 35.71 | 79.94 | 16.59 |

(b) Photovoltaic characteristics of the $MoO_x$/$n$-Si solar cells with different affinities of the $SiO_x$(Mo)1 layer

| Affinity of $SiO_x$(Mo)1 (eV) | $V_{oc}$ (mV) | $J_{sc}$ (mA·cm$^{-2}$) | FF (%) | $\eta$ (%) |
|---|---|---|---|---|
| 3.45 | 581.1 | 35.72 | 81.81 | 16.98 |
| 3.50 | 581.1 | 35.72 | 81.45 | 16.91 |
| 3.55 | 581.3 | 35.72 | 79.10 | 16.43 |
| 3.60 | 582.6 | 35.72 | 68.99 | 14.36 |

Table 3: Photovoltaic characteristics of the $MoO_x$/$n$-Si solar cells with different concentrations of the negative charge centers.

| Na | $V_{oc}$ (mV) | $J_{sc}$ (mA·cm$^{-2}$) | FF (%) | $\eta$ (%) |
|---|---|---|---|---|
| $1 \times 10^{16}$ | 581.10 | 35.72 | 81.45 | 16.91 |
| $1 \times 10^{17}$ | 581.10 | 35.72 | 81.45 | 16.91 |
| $1 \times 10^{18}$ | 581.20 | 35.72 | 81.48 | 16.91 |
| $1 \times 10^{19}$ | 581.20 | 35.70 | 81.72 | 16.96 |
| $1 \times 10^{20}$ | 581.00 | 35.51 | 81.89 | 16.89 |

ion-correlated in the $a$-$SiO_x$(Mo)1 layer. Table 3 shows the photovoltaic parameters of the MSHJ devices with different negative charge center concentrations in the range of $1 \times 10^{15} - 1 \times 10^{19}$ cm$^{-3}$. Notably, the photovoltaic characteristics remained unchanged for the negative charge center concentrations below $1 \times 10^{16}$ cm$^{-3}$, which directly verified that the built-in field mainly originated from the work function difference between the $MoO_x$ (5.50 eV) and the $n$-Si (4.31 eV). To achieve high output performances of the device, the negative charge center concentrations should be controlled in the range of $1 \times 10^{16} - 10^{18}$ cm − 3, meaning a wide adjustable range of fabricating process. These negative charge centers repel electron to the back side of solar cells so as to obtain large $J_{sc}$.

The simulation results showed that the $a$-$SiO_x$(Mo) layer was a large band gap (~2.30 eV) semiconductor material with good quantum tunneling and field-effect passivation. Furthermore, the results clarified that the barrier height was lowered by the included molybdenum ions, increasing the quantum tunneling probability. Furthermore, the negative charge centers in the $a$-$SiO_x$(Mo) layer, which was introduced by the included molybdenum ions and oxygen vacancies, played a crucial role in the good field-effect passivation. The clarification of the interfacial physical mechanism of the MSHJ solar cells enabled a better understanding of the nature of device physics. We investigated an a-$SiO_x$(In) interlayer that formed naturally between ITO and an $n$-Si substrate [17, 22, 25–27] during the growth of an ITO film on an $n$-Si wafer. The $a$-$SiO_x$(In) interlayer also played multiple roles in the ITO/$n$-Si heterojunction solar cell and helped produce an outstanding photovoltaic performance. We surmised that the $a$-$SiO_x$ interlayer included another specific transition metal oxide, for example, $VO_x$ or $WO_x$, which might also form a large energy band gap semiconductor material with a good passivation effect, a high tunneling possibility, and selective contacts.

*3.4. Electronic Structure and Roles of the Interfacial Region.* The device model revealed that there was a strong inversion layer ($p^+$) at the surface of the $n$-Si substrate because of the difference between the work functions of $MoO_x$ and $n$-Si, as shown in Figure 4. Such an inversion layer pushed the $p$/$n$ homojunction, which was the origin of the built-in field on the surface of $c$-Si. The calculated energy band structure of the interfacial region at equilibrium is shown in Figure 4. A strong $p$-type inversion layer with a thickness of approximately 200 nm existed near the surface of the $n$-Si absorber. Additionally, the simulation showed that there was an energy band bending of 0.81 eV, limiting the $V_{oc}$ value of the $MoO_x$/$n$-Si heterojunction on the surface of the Si substrate. A $V_{oc}$ value is usually correlated with a built-in potential ($V_{bi}$). For the fabricated device, a $V_{bi}$ value of 0.67 V was obtained, as derived from the $1/C^2$–$V$ curve at room temperature,

assuming an abrupt junction, as shown in Figure 5. It was clear that the measured value of 0.67 V was close to but smaller than the simulated value of 0.81 V. Considering the other factors of the fabricated device [28, 29], the simulated energy band structure essentially matches that of the fabricated device.

Based on the energy band structure, we could see that the valence band and conduction band offsets were 0.46 eV and 0.71 eV, respectively. Both energy barriers induced by the band offsets and the electric field at the interface could separate electron-hole pairs due to the high degree of band bending [30, 31]. In our device, quantum tunneling played an important role in the explanation of the charge carrier transport. The tunneling probability for the charge carriers was strongly influenced by the height of the barrier, the thickness of the barrier, the barrier shape, and many other factors [25, 32–36]. The valence band offset of 0.46 eV offered a relatively low potential barrier for the holes. Hence, the tunneling probability for the holes increased significantly. As expected, the increased tunneling probability for the holes could directly lead to a higher $J_{sc}$.

Furthermore, the conduction band offset of 0.71 eV resulted in a high potential barrier for the electrons, restricting their transport. Moreover, the negative charge centers repelled electrons to the backside of $c$-Si due to field-effect passivation. We found that the $SiO_x$(Mo) layer was a desirable material that was suitable for hole transport while preventing electron transport, thus obtaining a high

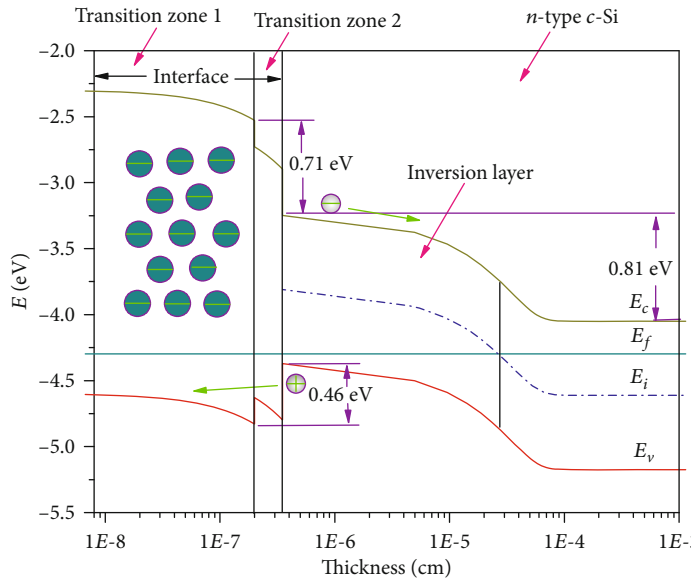


Figure 4: Energy band diagram at equilibrium.

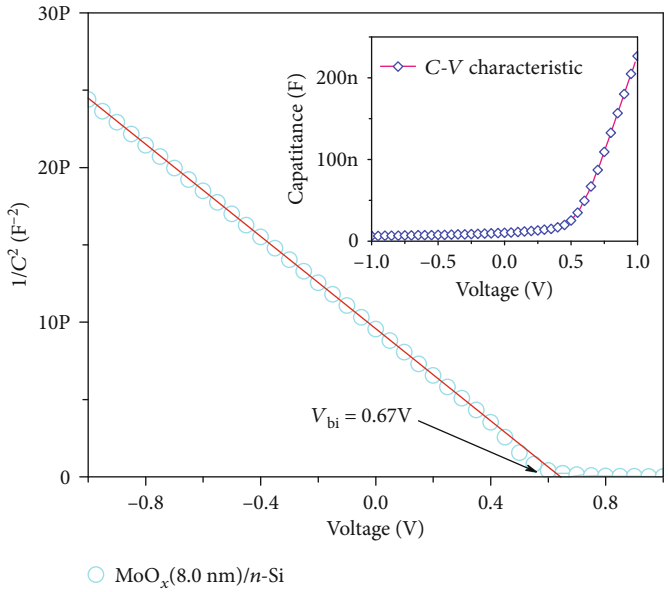


Figure 5: $1/C^2$ versus voltage plot of the $MoO_x$/n-Si device.

$J_{sc}$. Therefore, the $a$-$SiO_x$(Mo) interfacial layer offered a strong field-effect passivation and high quantum tunneling probability, which was of great significance for the output performance of MSHJ solar cells. The $a$-$SiO_x$(Mo) interlayer enabled holes to be more easily transported by assisted tunneling, and it repelled electrons on the other side of the layer with Coulombic force, thereby indicating that it was a promising material for heterojunction solar cells. Liu et al. investigated the band arrangement and charge transfer when the interfacial interaction varied on the $BiVO_4/WO_3$ heterostructure semiconductor material [37]. One can find that the charge transfer internal mechanism of the interfacial layer in the heterojunction needs to explore furthermore. This interfacial material of MSHJ is open to further research; although, we could independently prepare an $a$-$SiO_x$(Mo) layer at the time of this research.

## 4. Conclusions

By employing a simple process, we fabricated a $MoO_x$/$n$-Si solar cell that achieved good performance with an $\eta$ of 13.94%, an open-circuit voltage of 569.96 mV, a short-circuit current density of 32.10 mA·cm$^{-2}$, and a high FF of 76.21%. We found that a 3.5 nm ternary-like hybrid layer of $a$-$SiO_x$(Mo) formed between the $MoO_x$ and the $n$-Si

substrate, and that the hybrid layer might have played a vital role in the good performance of the MSHJ solar cells. The subsequent simulation results demonstrated that this interfacial layer $SiO_x$(Mo)1 was a Mo-based semiconductor material with a wide optical band gap of ~2.30 eV and negative charge centers with densities in the range of $10^{11}$-$10^{12}$ $cm^{-2}$. The interfacial layer $SiO_x$(Mo)2 played the role of passivation in the $MoO_x$/*n*-Si device. The negative charge centers played dual roles in both the quantum tunneling and field-effect passivation processes, resulting in the excellent transport characteristics of the majority charge carriers and the effective suppression of the minority charge carrier recombination. The improved performance, the clarification of the physical mechanism, and the superiority of the fabrication process indicated that the MSHJ solar cells would have appealing prospects in mass production. Finally, the clarification of the MSHJ device physics will effectively help in understanding the role of the interfacial layer and improving the output performance of these devices. Based on the above analysis, we expect that *a*-$SiO_x$ material including transition metal oxides, such as $VO_x$, with excellent passivation, high tunneling possibility, and selective contacts, may become an appealing material for heterojunction solar cells.

## Data Availability

Please contact with this email xmsong@jou.edu.cn, if you need the data supporting about this article.

## Conflicts of Interest

The authors declare that they have no conflicts of interest.

## Acknowledgments

This work was partly supported by the National Natural Science Foundation of China (Nos. 61874070, 61774069, 61674099, and 61274067), Major Projects of Jiangsu Education Department (No. 20KJA430013), R&D Foundation of SHU-SOENs PV Joint Lab (No. SS-E0700601), and Lianyungang "Haiyan Plan" (No. 2020-QD-010).

## References

[1] C. Waldauf, M. Morana, P. Denk et al., "Highly efficient inverted organic photovoltaics using solution based titanium oxide as electron selective contact," *Applied Physics Letters*, vol. 89, no. 23, article 233517, 2006.

[2] E. J. Juarez-Perez, M. Wubler, F. Fabregat-Santiago et al., "Role of the selective contacts in the performance of lead Halide Perovskite solar cells," *Journal of Physical Chemistry Letters*, vol. 5, no. 4, pp. 680–685, 2014.

[3] C. Battaglia, X. Yin, M. Zheng et al., "Hole selective MoOx contact for silicon solar cells," *Nano Letters*, vol. 14, no. 2, pp. 967–971, 2014.

[4] C. Battaglia, S. M. de Nicolás, S. De Wolf et al., "Silicon heterojunction solar cell with passivated hole selective MoOxcontact," *Applied Physics Letters*, vol. 104, no. 11, article 113902, 2014.

[5] M. Bivour, J. Temmler, H. Steinkemper, and M. Hermle, "Molybdenum and tungsten oxide: high work function wide band gap contact materials for hole selective contacts of silicon solar cells," *Solar Energy Materials and Solar Cells*, vol. 142, pp. 34–41, 2015.

[6] J. Bullock, A. Cuevas, T. Allen, and C. Battaglia, "Molybdenum oxide MoOx: a versatile hole contact for silicon solar cells," *Applied Physics Letters*, vol. 105, no. 23, article 232109, 2014.

[7] T. Yang, W. Ming, C. Yan, H. Fei, and C. Yong, "Polymer solar cells with a low-temperature-annealed sol-gel-derived MoOx film as a hole extraction layer," *Advanced Energy Materials*, vol. 2, no. 5, pp. 523–527, 2012.

[8] M. Zhang, Irfan, H. Ding, Y. Gao, and C. W. Tang, "Organic Schottky barrier photovoltaic cells based on MoOx/C60," *Applied Physics Letters*, vol. 96, no. 18, article 183301, 2010.

[9] S. Yanming, C. J. Takacs, S. R. Cowan et al., "Efficient, air-stable bulk heterojunction polymer solar cells using MoO(x) as the anode interfacial layer," *Advanced Materials*, vol. 23, pp. 2226–2230, 2011.

[10] H. D. Um, N. Kim, K. Lee, I. Hwang, J. H. Seo, and K. Seo, "Dopant-free all-back-contact Si nanohole solar cells using MoOx and LiF films," *Nano Letters*, vol. 16, no. 2, pp. 981–987, 2016.

[11] F. Li, Z. Sun, Y. Zhou et al., "Lithography-free and dopant-free back-contact silicon heterojunction solar cells with solution-processed TiO2 as the efficient electron selective layer," *Solar Energy Materials and Solar Cells*, vol. 203, article 110196, 2019.

[12] M. Bivour, S. Schröer, and M. Hermle, "Numerical analysis of electrical TCO / a-Si:H(p) contact properties for silicon heterojunction solar cells," *Energy Procedia*, vol. 38, pp. 658–669, 2013.

[13] J. Geissbühler, J. Werner, S. Martin de Nicolas et al., "22.5% efficient silicon heterojunction solar cell with molybdenum oxide hole collector," *Applied Physics Letters*, vol. 107, no. 8, article 081601, 2015.

[14] R. Varache, C. Leendertz, M. E. Gueunier-Farret, J. Haschke, D. Muñoz, and L. Korte, "Investigation of selective junctions using a newly developed tunnel current model for solar cell applications," *Solar Energy Materials and Solar Cells*, vol. 141, pp. 14–23, 2015.

[15] D. Chen, M. Gao, Y. Wan, Y. Li, H. Guo, and Z. Ma, "Electronic structure of molybdenum-involved amorphous silica buffer layer in $MoO_x$/n-Si heterojunction," *Applied Surface Science*, vol. 473, pp. 20–24, 2019.

[16] M. Gao, D. Chen, B. Han et al., "Bifunctional hybrid a-SiOx(Mo) layer for hole-selective and Interface passivation of highly efficient MoOx/a-SiOx(Mo)/n-Si heterojunction photovoltaic device," *ACS Applied Materials & Interfaces*, vol. 10, no. 32, pp. 27454–27464, 2018.

[17] Y. Li, B. C. Han, M. Gao et al., "A concise way to estimate the average density of interface states in an ITO- $SiO_{-x-}$ /n-Si heterojunction solar cell," *Applied Surface Science*, vol. 416, pp. 432–438, 2017.

[18] S. Zhong, X. Hua, and W. Shen, "Simulation of high-efficiency crystalline silicon solar cells with homo–hetero junctions," *IEEE Transactions on Electron Devices*, vol. 60, no. 7, pp. 2104–2110, 2013.

[19] L. Zhao, C. L. Zhou, H. L. Li, H. W. Diao, and W. J. Wang, "Design optimization of bifacial HIT solar cells on p-type silicon substrates by simulation," *Solar Energy Materials & Solar Cells*, vol. 92, no. 6, pp. 673–681, 2008.

[20] S. M. Sze and K. K. Ng, *Metal-Semiconductor Contacts*, John Wiley & Sons, Inc., 2006.

[21] A. Froitzheim, K. Brendel, L. Elstner, W. Fuhs, K. Kliefoth, and M. Schmidt, "Interface recombination in heterojunctions of amorphous and crystalline silicon," *Journal of Non-Crystalline Solids*, vol. 299-302, pp. 663–667, 2002.

[22] X. M. Song, M. Gao, Z. G. Huang et al., "Interface properties of ITO/n-Si heterojunction solar cell: quantum tunneling, passivation and hole-selective contacts," *Solar Energy*, vol. 173, pp. 456–461, 2018.

[23] G. L. Araujo and E. Sánchez, "Analytical expressions for the determination of the maximum power point and the fill factor of a solar cell," *Solar Cells*, vol. 5, no. 4, pp. 377–386, 1982.

[24] N. Tomozeiu, *Silicon oxide (SiOx, 0&ltx&lt2): a challenging material for optoelectronics*, INTECH, 2011.

[25] H. W. Du, J. Yang, Y. H. Li, F. Xu, J. Xu, and Z. Q. Ma, "Preparation of ITO/SiOx/n-Si solar cells with non-decline potential field and hole tunneling by magnetron sputtering," *Applied Physics Letters*, vol. 106, no. 9, article 093508, 2015.

[26] M. Gao, Y. Wan, Y. Li et al., "Effective passivation and tunneling hybrid a-SiOx(in) layer in ITO/n-Si heterojunction photovoltaic device," *ACS Applied Materials & Interfaces*, vol. 9, no. 20, pp. 17565–17575, 2017.

[27] Y. Z. Wan, M. Gao, Y. Li et al., "Potentiality of delocalized states in indium-involved amorphous silicon oxide," *Applied Physics Letters*, vol. 110, no. 21, article 213902, 2017.

[28] J. C. Blakesley and D. Neher, "Relationship between energetic disorder and open-circuit voltage in bulk heterojunction organic solar cells," *Physical Review B*, vol. 84, no. 7, 2011.

[29] C. Xiong, R.-H. Yao, and K.-W. Geng, "Photovoltage analysis of a heterojunction solar cell," *Chinese Physics B*, vol. 20, no. 5, article 057302, 2011.

[30] S. De Wolf, A. Descoeudres, Z. C. Holman, and C. Ballif, "High-efficiency silicon heterojunction solar cells: a review," *Green*, 2012.

[31] A. Cheknane, "Analytical modelling and experimental studies of SIS tunnel solar cells," *Journal of Physics D: Applied Physics*, vol. 42, no. 11, article 115302, 2009.

[32] H. C. Card and E. S. Yang, "MIS-Schottky theory under conditions of optical carrier generation in solar cells," *Applied Physics Letters*, vol. 29, no. 1, pp. 51–53, 1976.

[33] S. J. Fonash, "The role of the interfacial layer in metal–semiconductor solar cells," *Journal of Applied Physics*, vol. 46, no. 3, pp. 1286–1289, 1975.

[34] Y. T. Hou, M. F. Li, Y. Jin, and W. H. Lai, "Direct tunneling hole currents through ultrathin gate oxides in metal-oxide-semiconductor devices," *Journal of Applied Physics*, vol. 91, no. 1, pp. 258–264, 2002.

[35] J. Kang, Y.-H. Kim, J. Bang, and K. J. Chang, "Direct and defect-assisted electron tunneling through ultrathinSiO2layers from first principles," *Physical Review B*, vol. 77, no. 19, 2008.

[36] M. Lenzlinger and E. H. Snow, "Fowler-Nordheim tunneling into thermally grown SiO2," *Journal of Applied Physics*, vol. 40, no. 1, pp. 278–283, 1969.

[37] Y. Liu, G.-J. Zhao, J.-X. Zhang, F.-Q. Bai, and H.-X. Zhang, "First-principles investigation on the interfacial interaction and electronic structure of BiVO4/WO3 heterostructure semiconductor material," *Applied Surface Science*, vol. 549, article 149309, 2021.